

# Dielectrophoretic Trapping Without Embedded Electrodes

E. B. Cummings, A. K. Singh

Sandia National Laboratories, P. O. Box 969, Livermore, CA, U.S.A.

## ABSTRACT

We observe dielectrophoretic effects in mixed electrokinetic and dielectrophoretic flows in uniform arrays of posts. Above a threshold applied electric field, flowing filaments of concentrated and rarefied particles appear in the flow. Above a higher-threshold applied field, zones of highly concentrated, immobilized particles appear. At the lower and higher thresholds, dielectrophoresis apparently begins to dominate diffusion and advection/electrokinetics, respectively. The patterns of filaments and trapped zones depend dramatically on the angle of the array with respect to the mean applied electric field and the shape of the posts in the array.

**Keywords:** Dielectrophoresis, Electroosmosis, electrophoresis, electrokinetic flow, patterned bed, microarrays, trapping, latex microspheres, microfluidics, separations

## 1. INTRODUCTION

Dielectrophoresis (DEP) is the motion of particles toward or away from regions of high electric-field intensity.<sup>1,2</sup> This motion is produced by the action of an electric field on dipole moments induced in the particle and the suspending fluid by the electric field. If the induced dipole moment of the particle is greater than that of the fluid, the particle is said to exhibit “positive dielectrophoresis” and experiences a force toward regions of high electric field intensity. “Negative dielectrophoresis” occurs when the fluid is more polarizable than the suspended particle and the particles are forced away from high-field regions. Dielectrophoresis has captured much interest recently because it is an effective way to trap, manipulate, and separate particles ranging from DNA strands to blood cells and larger particles.<sup>3–9</sup> Most implementations of dielectrophoresis utilize embedded electrodes to produce field concentrations. Moreover, the applied fields are nearly always purely alternating current (AC).

In this study, we present direct-current (DC) dielectrophoretic effects on particle concentration in electrically driven flows through uniformly patterned arrays of insulating posts. In these flows, we observe two phenomena: dielectrophoretic “filamenting,” in which flowing filaments of low and high particle concentration appear in the flow and “trapping,” in which zones of reversibly immobilized particles appear. The former effect occurs when the dielectrophoresis overcomes diffusion; the latter occurs when dielectrophoresis overcomes advection and electrophoresis (EP). We observe dramatic dependence of the patterns of filamenting and trapping on the orientation of arrays with respect to the mean applied electric field and on the shape of the posts in the arrays.

## 2. THEORY OF DIELECTROPHORESIS

The theory of dielectrophoresis has been well developed.<sup>1,2</sup> A particle in an electric field experiences a dielectrophoretic potential that is proportional to the local electric field intensity,  $\mathbf{E} \cdot \mathbf{E} = \nabla\phi \cdot \nabla\phi$ , where  $\mathbf{E}$  and  $\phi$  are the electric field and potential, respectively. The dielectrophoretic flow velocity of a particle,  $\mathbf{u}_{dep}$ , can be constitutively related to the gradient of this DEP potential field via the dielectrophoretic mobility,  $\mu_{dep}$ ,

$$\mathbf{u}_{dep} = -\mu_{dep}\nabla(\mathbf{E} \cdot \mathbf{E}) \quad (1)$$

This mobility is a function of the physical and chemical properties of the particle and suspending fluid. In the following sections, the concentration of particles is assumed to be sufficiently dilute that interparticle interactions can be ignored. This approximation clearly does not hold in regions that are dense with trapped particles, but is justifiable elsewhere in the flows under consideration. The effects of interest in this study are not “particle to particle” DEP interactions like chain formation, but rather “electric-field-gradient on suspended-particle” interactions.

Assume surfaces bounding the flow are insulating and have a uniform electroosmotic (EO) mobility,  $\mu_{eo}$ . Assume the flow channels are geometrically much larger than the Debye length of the fluid. Further assume that the fluid

---

Correspondence should be directed to ebcummi@sandia.gov

has uniform electrical properties and the applied electric field is steady. Then, sufficiently far away from electrodes, the fluid's electric,  $\mathbf{E}$ , and electroosmotic velocity,  $\mathbf{u}_{eo}$ , fields are everywhere related by the EO mobility and are the gradient of a scalar potential  $\phi$  that is a solution of the Laplace equation.<sup>10</sup>

$$\mathbf{u}_{eo} = \mu_{eo}\mathbf{E} = \mu_{eo}\nabla\phi; \quad \nabla^2\phi = 0 \text{ in } V; \quad \nabla\phi \cdot \hat{\mathbf{e}}_{\mathbf{n}} = 0 \text{ on } S, \quad (2)$$

where  $V$  and  $S$  denote the volume and the insulating-surface regions, respectively and  $\hat{\mathbf{e}}_{\mathbf{n}}$  is the unit vector normal to the surface. The electrophoretic mobility relates the velocity of a particle with respect to the surrounding fluid to the electric field,

$$\mathbf{u}_{ep} = -\mu_{ep}\mathbf{E}. \quad (3)$$

The combined effect of electroosmosis and electrophoresis on particle motion relative to a fixed channel can be described by an electrokinetic mobility,  $\mu_{ek}$ ,

$$\mathbf{u}_{ek} = -\mu_{ek}\mathbf{E} = \mathbf{u}_{eo} + \mathbf{u}_{ep} = (\mu_{eo} - \mu_{ep})\mathbf{E}. \quad (4)$$

This result is later used in the calculation of electrokinetic flow streamlines and the combined EK and DEP potential,  $\psi$ ,

$$\psi = \phi + \frac{\mu_{dep}}{\mu_{ek}}\nabla\phi \cdot \nabla\phi. \quad (5)$$

For dilute, creeping flows in insulating channels, the particle concentration flux,  $\mathbf{j}$ , including diffusion, advection, electrokinesis, and dielectrophoresis is

$$\mathbf{j} = -D\nabla c + c[\mathbf{u} - \mu_{ek}\mathbf{E} + \mu_{dep}\nabla(\mathbf{E} \cdot \mathbf{E})], \quad (6)$$

where  $D$  is the diffusivity and  $\mathbf{u}$  is the non-electrokinetic component of the velocity. By continuity, the rate of change of the concentration is equal to the divergence of the concentration flux,

$$\frac{\partial c}{\partial t} = \nabla \cdot \mathbf{j}. \quad (7)$$

If the particle-concentration field  $c$  is uniform before applying an electric field, (7) is

$$\frac{\partial c}{\partial t} = \mu_{dep}c\nabla \cdot \nabla(\mathbf{E} \cdot \mathbf{E}), \quad (8)$$

initially after applying the field. The advection and EK terms disappear by continuity and terms proportional to gradients of  $c$  are dropped. Consequently, dielectrophoresis is the only effect of the ones considered that produces a particle-concentration gradient in an initially uniform fluid.

### 3. EXPERIMENTAL APPARATUS

The experimental apparatus is shown schematically in Figure 1. Experiments were conducted on microflows in a microfluidic circuit consisting of patterned channels isotropically etched  $\sim 7\text{-}\mu\text{m}$  deep in glass with a thermally bonded glass cover. The microfluidic circuit is reversibly sealed to a test fixture via a vacuum chuck. This fixture provides 16 open, 1-ml fluid reservoirs with embedded gold ring electrodes. A high-voltage power supply (Stanford Research Systems, PS350) is used to apply electric fields. The fluid is a suspension of fluorescent nanospheres (Molecular Probes yellow-green, 200-nm, carboxylate-modified fuospheres) in an aqueous 1-mM phosphate-buffered saline solution at pH 7.7. These neutrally buoyant nanospheres are labeled with a highly fluorescent dye similar to fluorescein. The microflows are imaged by an LED-illuminated, inverted, three-video-camera epifluorescence microscope. A ring of 24 blue LEDs (Nichia, NSPB300A) flood illuminates the sample with light having a peak wavelength of  $\sim 470$  nm. A  $10\times$  microscope objective ( $O1$ ) images a  $\sim 520\text{-}\mu\text{m} \times 390\text{-}\mu\text{m}$  region of the circuit onto cameras  $C1$ ,  $C2$ , and  $C3$ . Dichroic mirror  $M1$  reflects fluorescence in the wavelength range below  $\sim 550$  nm into an emission filter  $F1$  which further limits the signal wavelength range to 500–530 nm. The filtered signal falls on a video-rate monochromatic 1/2-inch CCD camera (Cohu 4910,  $C1$ ). Cameras  $C2$  and  $C3$  support secondary diagnostics.

The microfluidic circuit contains 72 different patterned arrays arranged in 12 sets of independently addressable subcircuits. Each subcircuit consists of 6 separate patterned arrays, each of which is straddled by two open calibration channels. The array porosity, angle-of-attack, and packing arrangement as well as the post shape and size systematically vary across the circuit.

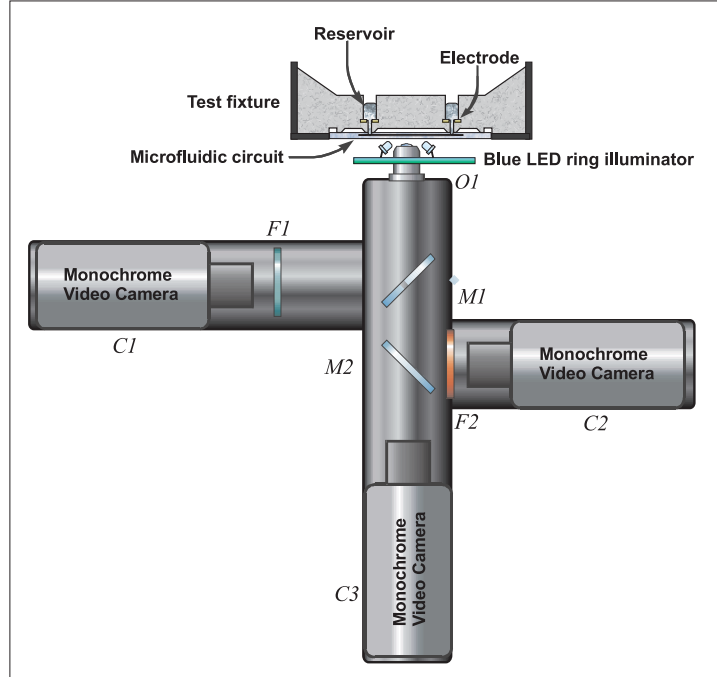


**Figure 1.** Schematic diagram of the experimental apparatus. A custom test fixture provides fluidic reservoirs and electrical interconnects to the microfluidic circuit. Camera  $C1$  captures fluorescence from particles suspended in the fluid within the micropatterned arrays. The other two cameras support other diagnostics.

#### 4. FILAMENTARY DIELECTROPHORESIS

Because the dielectrophoretic effect is of second order in the applied electric field, it is negligible at suitably low applied fields. In this limit, the dominant particle-transport mechanisms are electrokinesis and diffusion. As discussed earlier, advection and electrokinesis do not induce changes in particle concentration for a fluid having a dilute, initially uniform particle concentration. Diffusion and hydrodynamic dispersion overwhelm weak dielectrophoresis so no appreciable spontaneous particle concentration gradients form. However, the behavior of particles in mixed dielectrophoretic and advective/electrokinetic flows changes qualitatively near two threshold applied electric fields: a threshold in which dielectrophoresis begins to dominate diffusion and a threshold in which dielectrophoresis becomes comparable to and greater than advection and electrokinesis.

Assuming, as is typically the case, the Peclet number of the particles in the flow is greater than unity, the former threshold occurs at a lower applied electric field than the latter. Above this lower threshold, “filaments” with enhanced or depleted particle concentration appear primarily along flow streamlines. These filaments form when dielectrophoresis begins to produce concentration gradients in the flow. Unlike concentration gradients tangent to streamlines, gradients normal to streamlines are not distorted or dispersed hydrodynamically. Therefore, gradients normal to streamlines can persist even when the dielectrophoretic effect is too weak to overcome dispersion, so the concentration fields satisfy

$$\nabla c \cdot (\mathbf{u} + \mathbf{u}_{ek}) \ll \|\nabla c \times (\mathbf{u} + \mathbf{u}_{ek})\|, \quad (9)$$

where, again,  $\mathbf{u}$  accounts for non-electrokinetic components of the flow velocity and  $\mathbf{u}_{ek}$  accounts for both electroosmosis and electrophoresis. Expression (9) allows one to analyze filamentary dielectrophoresis using a boundary-layer approach. In special cases, e.g., in well-developed flows in uniform periodic arrays, one may approximate that

$$\nabla c \cdot (\mathbf{u} + \mathbf{u}_{ek}) \simeq 0. \quad (10)$$

In this approximation, constant-concentration filaments form along streamlines so that the osmotic pressure of the particles balances the effective mean dielectrophoretic potential along the streamline.

Figures 2–6 show images of filamentary dielectrophoresis in an otherwise purely electrokinetic flow. The images are approximately 1-s time averages. The gray scale of the image shows the relative intensity of the particle fluorescence and is thus a measure of the concentration of the particles. The thin, bright border around each post is strong specular reflection of the illumination light that leaks through the filters and is not a fluorescence signal. All flows are from top to bottom.

Figure 2 shows the particle-concentration variation in a flow past the end of a uniform square array of circular posts. The posts are arranged on  $63\text{-}\mu\text{m}$  centers, with  $33\text{-}\mu\text{m}$  diameters. The angle of the array is  $0.0^\circ$ , meaning the mean applied field of  $\sim 25\text{V}/\text{mm}$ , or  $1.6\text{ V}/\text{row}$  is closely aligned with columns of posts. The array is 56 posts long (in the flow direction) and 16 posts wide. Electrokinetic flow streamlines are superimposed on the image. These streamlines are produced using a potential flow solver that can generate a computational grid from an image of the flow-boundary geometry. The bright patches generally toward the right of the image are fluorescent agglomerates that had previously stuck to the channel surface.

The particle concentration varies little in the core flow between the post columns. Approaching the columns, the concentration increases several-fold. Near the stagnation streamline down the center of the column, the concentration dips significantly. This pattern of particle concentration persists as the streamlines leave the post array, supporting the approximation (9) everywhere and (10) within the post array.

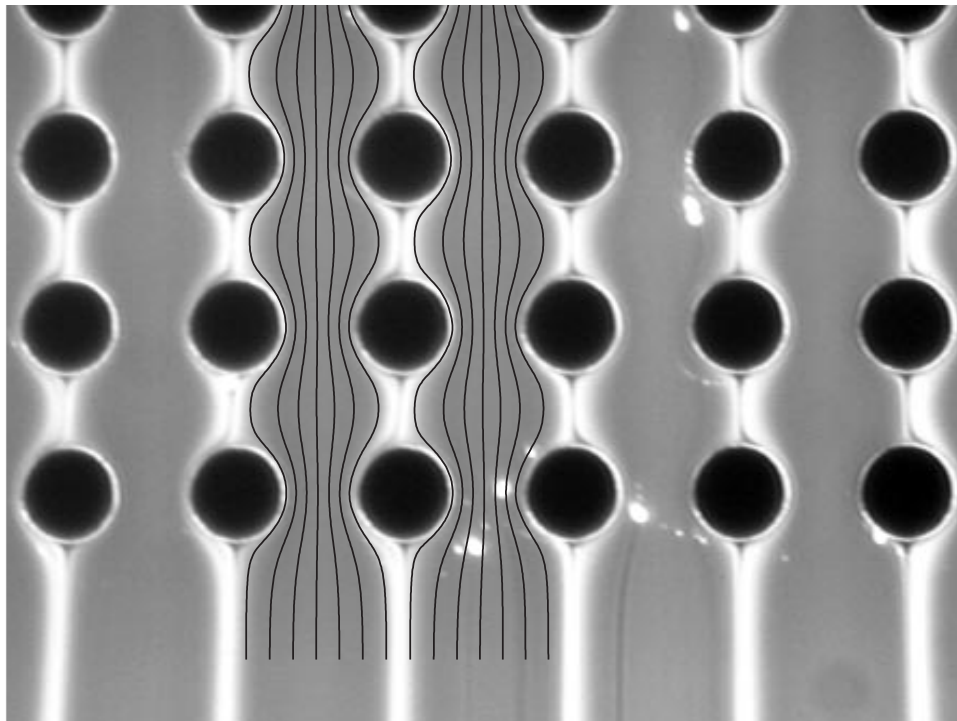


**Figure 2.** Fluorescence image of particle flow past a square array of  $33\text{-}\mu\text{m}$  circular posts at a  $0.0^\circ$  angle with respect to the mean applied field,  $1.6\text{ V}/\text{row}$

Figure 3 shows the particle-concentration variation in a flow past the end of a uniform square array of square posts arranged on  $63\text{-}\mu\text{m}$  centers, with  $36\text{-}\mu\text{m}$  sides. The properties of the array are otherwise the same as those of the previous array. The  $\sim 80\text{-V}/\text{mm}$  ( $5.0\text{ V}/\text{row}$ ) mean field is applied at an angle of  $1.6^\circ$  with respect to the array. This angle of attack produces filaments that are asymmetrical with respect to the post columns. Again, the filaments align with the calculated electrokinetic flow streamlines. In this case, the large stagnant regions of the flow between the posts are highly depleted of particles. There is no evidence of filaments having significantly enhanced concentration as seen in Fig. 2. In fact, the difference between these images is a striking demonstration of the importance of post shape in the dielectrophoretic behavior of an array.

Figure 4 shows the particle-concentration fields at the base of the same array as in Fig. 3 but with the electric



**Figure 3.** Fluorescence image of particle flow past a square array of  $36\text{-}\mu\text{m}$  square posts at  $1.6^\circ$  angle of attack with respect to the mean applied field,  $5.0\text{ V/row}$ .

field applied at  $2.3^\circ$  with respect to the array. The asymmetrical concentration gradient is dramatically steep toward the left of the post columns and relatively diffuse toward the right.

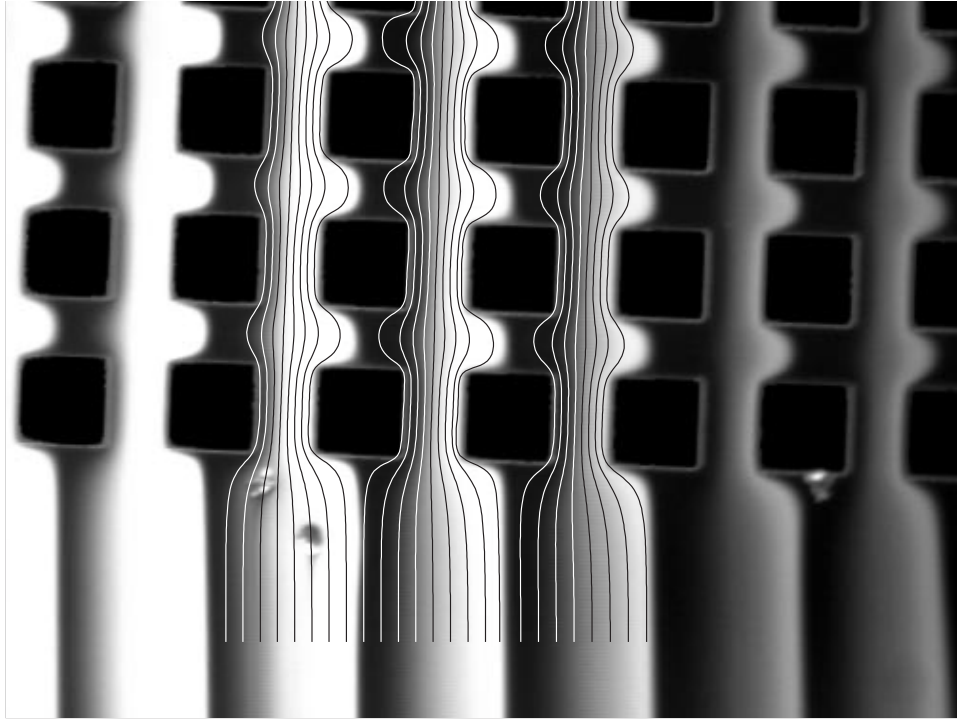
Figure 5 shows the particle-concentration field in the center of an array of posts with the same properties as those of Figs. 3 and 4 but with the array oriented at  $20.5^\circ$  degrees with respect to the applied electric field of  $\sim 80\text{ V/mm}$ . In this flow, the variation in concentration is much weaker than in the previous flows because of the limited cooperative effect of the posts. The concentration gradients are only weakly coherently enhanced by the array since the streamline patterns approximately repeat after an offset of 5 rows and 2 columns rather than the offset of approximately 1 row in the previous figures.

Figure 6 shows the particle-concentration field in the center of a square array similar to those in the previous figures but with an electric field of  $80\text{ V/mm}$  applied at a  $\sim 45.3^\circ$  angle with respect to the array. In this flow, the streamline pattern approximately repeats after an offset of 1 row and 1 column. The diagonal orientation of the square posts creates a large electric field concentration at the left and right vertices. The dielectrophoretic effect adds coherently in the array to produce a filament of high particle concentration that travels down the streamline at center of the channels. This effect significantly reduces the interactions of the particles with the posts. Similar arrays have been proposed and used<sup>11,12</sup> for electrochromatography, where sharply reduced surface interactions of positive dielectrophoretic molecules may affect separations.

The bright regions near the left and right vertices of the posts show the onset of particle trapping. As time progressed, these regions grew as shown in Fig. 9 in the next section.

## 5. TRAPPING DIELECTROPHORESIS

The second threshold in mixed dielectrophoretic and electrokinetic flows occurs at an applied electric field in which the local dielectrophoretic force exceeds the electrokinetic and hydrodynamic drag force. Above this threshold, regions appear where particles are “trapped” by the dielectrophoretic field. The number of particles in the trap grows in time until the applied field stops, the particles fill the region of the trap, or the presence of particles modifies the trap by perturbing the electric field.



**Figure 4.** Fluorescence image of particle flow past the same array as in Fig. 3 at  $2.3^\circ$  angle of attack with respect to the mean applied field, 5.0 V/row.

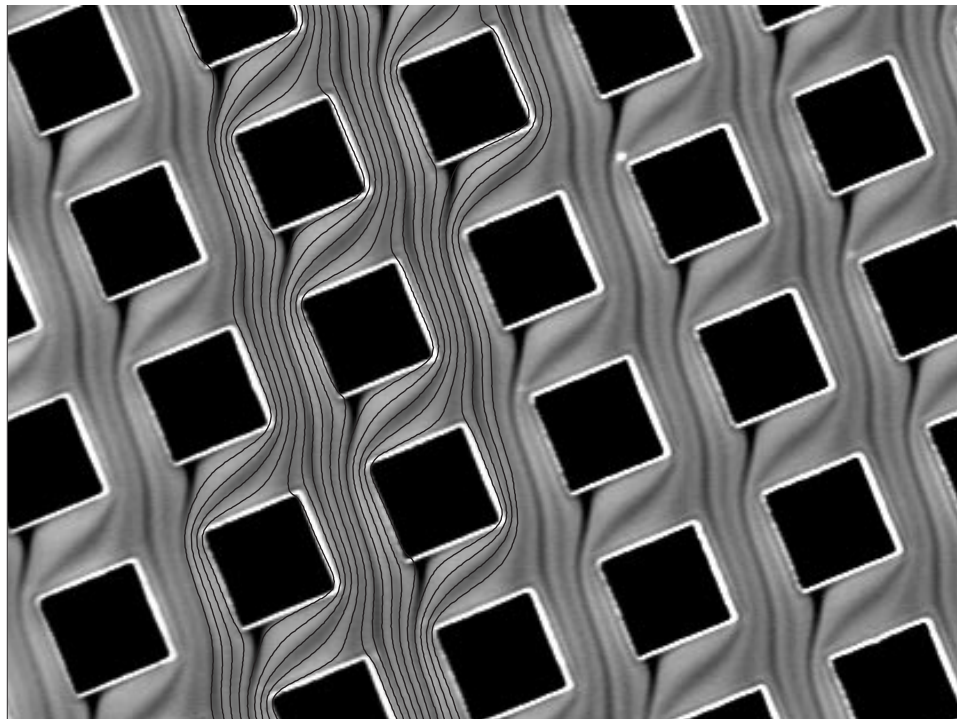


**Figure 5.** Fluorescence image of particle flow past a square array of square posts at  $20.5^\circ$  angle of with respect to the applied field of 80 V/mm.

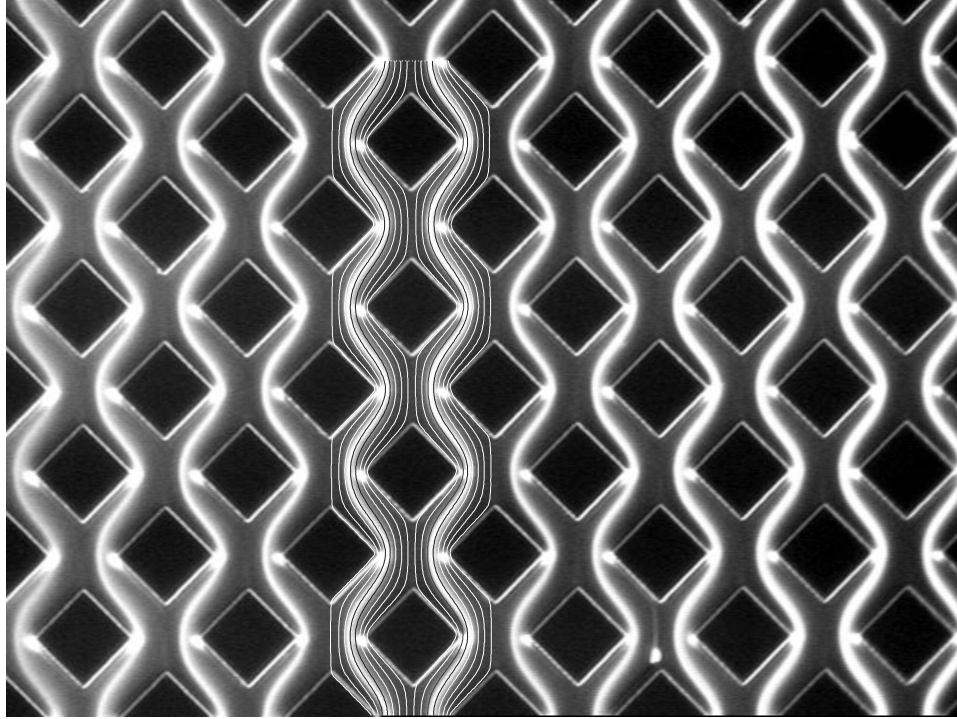


**Figure 6.** Fluorescence image of particle flow past a square array of  $36\text{-}\mu\text{m}$  square posts at  $45.3^\circ$  angle with respect to the applied field of  $80\text{ V/mm}$ .

Figure 7 shows a graphical representation of the combined electrokinetic and dielectrophoretic potential,  $\psi$  from (5), within a cell of three kinds of uniform arrays. The flow is from top to bottom. Isopotentials are lines of constant phase along a fringe. Adjacent fringes correspond to one tenth of the cell unit-potential difference. The potential difference across the cell, the size of the cell and the electrokinetic mobility of the particles are normalized to unity. Because of the practical absence of inertia, particles travel in paths normal to the isopotentials. The left-most images show the undisturbed electrokinetic potential within the arrays. The other images show the distortion of the combined EK and DEP potential of particles having a relative dielectrophoretic mobility of 0.0125, 0.025, and 0.05. Trapping zones (for positive dielectrophoretic particles) appear in the lower-left and right sides of the circular posts. Smaller zones appear for the on-axis square array. The  $45^\circ$  square array shows the formation of strong and sizable trapping zones even at low DEP mobility. The depth of the potential well of the traps is proportional to the number of fringes that curve around the well.

Figure 8 shows the flow in the interior of the array of Fig. 2 at an applied electric field of  $\sim 100\text{ V/m}$ . The bright regions to the lower left and right of the circular posts contain trapped particles. Relatively weak fluorescence from concentrated filaments are evident along the streamlines near the regions of trapped particles. This image was recorded after the trapped regions had apparently reached steady state, about 5 seconds after the electric-field forcing started. The zones where particles are trapped are consistent with the location of the wells in the combined potential fields in Fig. 7.

Figure 9 is from the same flow shown in Fig. 6. Figure 9 shows the particle concentration field 5 seconds after the electrical forcing started, a period of apparent steady state, while Fig. 6 was taken less than 1 second after the forcing started. The filaments of concentrated particles in Fig. 6 also appear in Fig. 9. In addition, new filaments down the stagnation streamlines appear, apparently produced by leakage from the trap. The zone of trapped particles is elongated alee of the post vertices compared to the location of the wells in Fig. 7. This disagreement could be a result of the disturbance in the electric and fluid-velocity fields produced by the trapped particles.

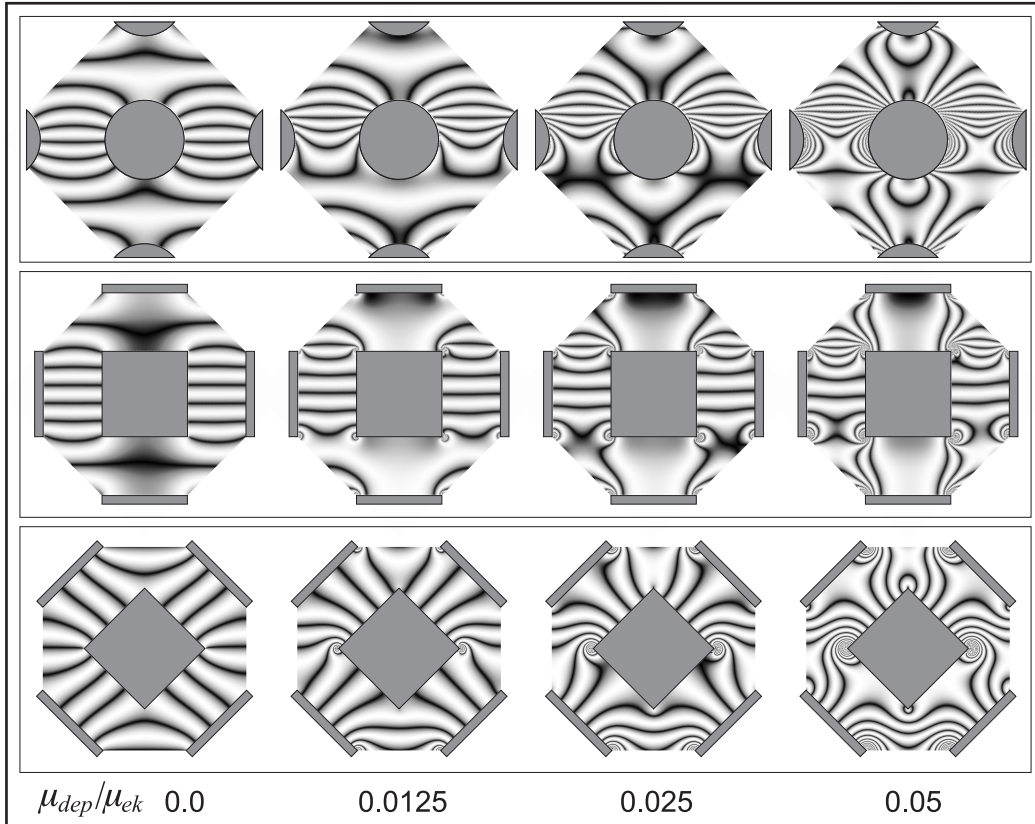


**Figure 7.** Combined electrokinetic and dielectrophoretic potential fields in cells of a uniform array vs. relative magnitude of the dielectrophoretic effect. The flow is from top to bottom.

## 6. CONCLUSIONS

We have demonstrated purely DC dielectrophoretic concentration, depletion, and trapping of particles in microfluidic systems with electrokinetic flow. The systems are noteworthy for their simplicity of fabrication: isotropic glass etching. No embedded electrodes or small/high-aspect-ratio structures are required to produce significant effects on particles of 200-nm diameter. These systems can be hot-embossed inexpensively into plastics and are amenable to other mass-fabrication techniques.

Filamentary dielectrophoresis can be used to enhance or deplete spatially the number density of particles in a stream, with applications to flow-through concentration or filtration. Furthermore, preferred streamlines or concentrated filaments temporally disperse the time of flight of particles down the array on the basis of their dielectrophoretic mobility. This dispersion can be used for separation by dielectrophoretic mobility. Trapping dielectrophoresis can reversibly concentrate particles to high density in zones of a flow-through system, also with applications to concentration, filtration, and separation.<sup>5,9</sup> Because dielectrophoresis is nonlinear in the applied electric field, the magnitude of the effect is tunable by simply changing the applied electric field (or the sinusoidal and constant components of the applied field in an AC/DC dielectrophoretic system).

The impact of the post shape and angle of the array with respect to the applied fields on the concentration fields is remarkable, with square posts producing essentially the opposite effect from circular posts. This observation supports the intuitive notion that the shape and arrangement of posts in an array can be optimized to enhance a particular behavior, something that is not possible in a randomly packed medium. As evidenced by Fig. 5, the magnitude of gradients produced dielectrophoretically decreases when there is little or no coherent forcing. Thus dielectrophoretic filamenting can be ignored in theoretical studies of particle transport and separations in random media, but this approximation is not necessarily justified in patterned or structured media.

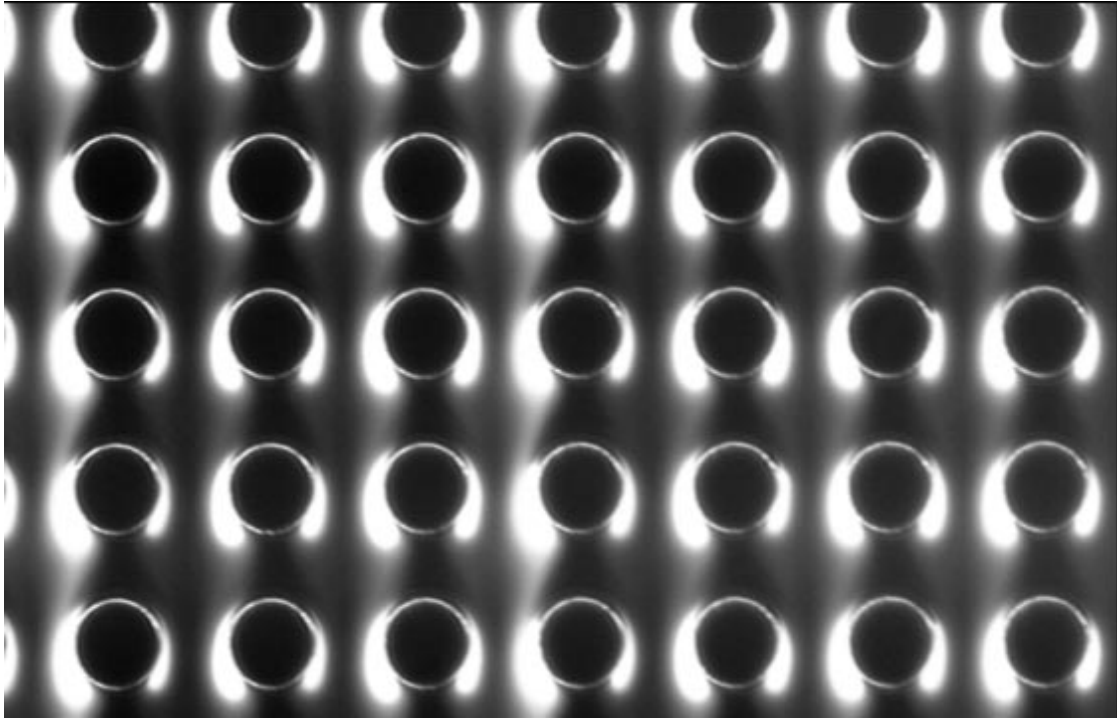


**Figure 8.** Fluorescence image of particle flow past a square array of  $33\text{-}\mu\text{m}$  circular posts at a slight angle with respect to the applied field of  $100\text{ V/mm}$ . This image shows the size of regions of trapped particles after the field has been applied for 5 seconds. The asymmetry of the regions is apparently caused by the angle of attack.

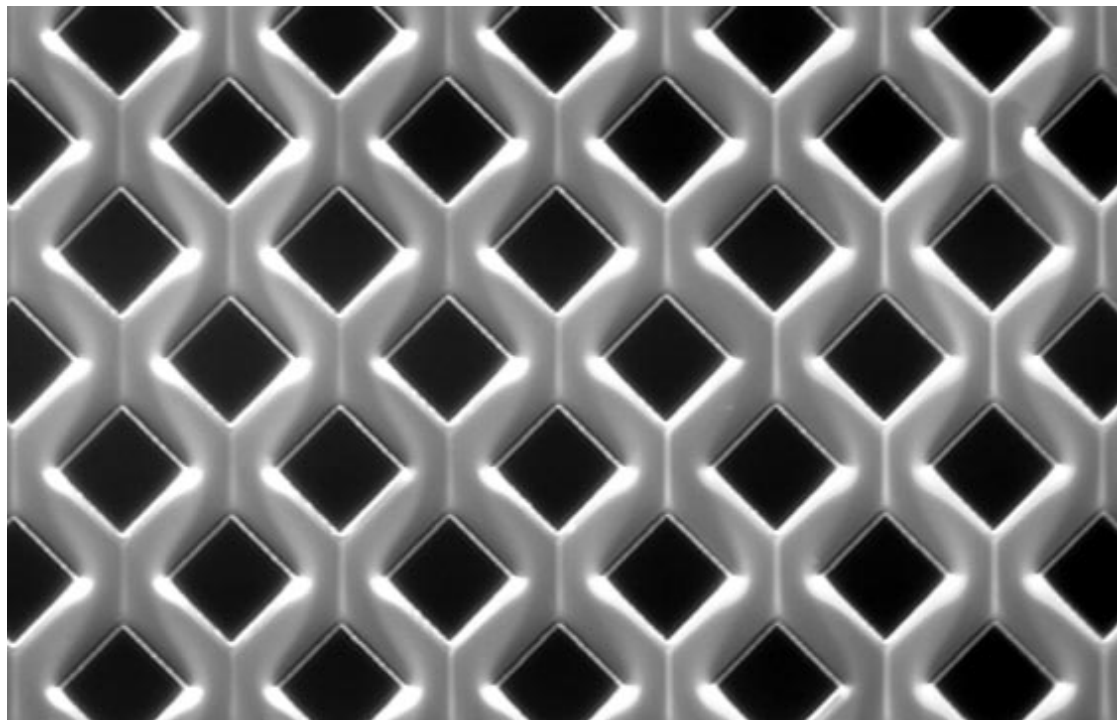


**Figure 9.** Fluorescence image of particle flow past a square array of  $36\text{-}\mu\text{m}$  square posts at a  $45.3^\circ$  angle to the applied field of  $80\text{ V/m}$ . This image shows an apparent steady-state after the field has been applied for 5 seconds.

## ACKNOWLEDGMENTS

This work was funded by a Sandia Engineering Sciences LDRD. Sandia is a multi-program laboratory operated by Sandia Corporation, a Lockheed-Martin company, for the United States Department of Energy under contract DE-AC04094AL85000.

## REFERENCES

1. H. A. Pohl, *Dielectrophoresis*, Cambridge University Press, Cambridge, 1978.
2. T. B. Jones, *Electromechanics of Particles*, Cambridge University Press, Cambridge, 1995.
3. P. R. C. Gascoyne, Y. Huang, R. Pethig, J. Vykoukal, and F. F. Becker, "Dielectrophoretic separation of mammalian-cells studied by computerized image-analysis," *Meas. Sci. & Tech.* **3**, pp. 439–445, 1992.
4. J. Cheng, E. L. Sheldon, L. Wu, A. Uribe, L. O. Gerrue, J. Carrino, M. J. Heller, and J. P. OConnell, "Preparation and hybridization analysis of dna/rna from e-coli on microfabricated bioelectronic chips," *Nature Biotechnology* **16**, pp. 541–546, 1998.
5. G. H. Markx and R. Pethig, "Dielectrophoretic separation of cells: continuous separation," *Biotechnology and Bioengineering* **45**, pp. 337–343, 1995.
6. N. G. Green and H. Morgan, "Dielectrophoretic investigations of sub-micrometre latex spheres," *J. Phys. D* **30**, pp. 2626–2633, 1997.
7. S. Fiedler, S. G. Shirley, T. Schnelle, and G. Fuhr, "Dielectrophoretic sorting of particles and cells in a microsystem," *Anal. Chem.* **70**, pp. 1909–1915, 1998.
8. H. Morgan, M. P. Hughes, and N. G. Green, "Separation of submicron bioparticles by dielectrophoresis," *Biophysical Journal* **77**, pp. 516–525, 1999.
9. G. H. Markx, J. Rousselet, and R. Pethig, "Dep-fff: Field-flow fractionation using non-uniform electric fields," *J. Liquid Chrom. & Rel. Tech.* **20**, pp. 2857–2872, 1997.
10. E. B. Cummings, S. K. Griffiths, R. H. Nilson, and P. H. Paul, "Conditions for similitude between the fluid velocity and electric field in electroosmotic flow," *Anal. Chem.* **72**, pp. 2526–2532, 2000.
11. B. He, N. Tait, and F. Regnier, "Fabrication of nanocolumns for liquid chromatography," *Anal. Chem.* **70**, pp. 3790–3797, 1998.
12. F. Regnier, "Microfabricated monolith columns for liquid chromatography : Sculpting supports for liquid chromatography," *HRC-J. High Res. Chrom.* **23**, pp. 19–26, 2000.